中国激光

对称负极芯片结构改善硅基激光器性能研究

马博杰[1]，王俊[1*]，刘昊[1]，江晨[1]，刘倬良[1]，翟浩[1]，李健[2]，明蕊[1]，葛庆[1]，林枫[1]，刘凯[1]，王琦[1]，韦欣[2]，黄永清[1]，任晓敏[1]

[1]北京邮电大学信息光子学与光通信国家重点实验室，北京 100876；

[2]中国科学院半导体研究所，北京 100083

摘要 本课题组设计了一种用于硅基外延激光器的对称负极芯片结构，与传统共面电极芯片结构相比，该结构大幅降低了硅基激光器的微分电阻，使激光器性能显著提升。采用该电极结构以及基于无偏角Si(001)衬底的量子点激光器外延材料进行了激光器芯片制作。芯片尺寸为1500 μm×50 μm的激光器的微分电阻仅为1.52 Ω，单面输出光功率可达70 mW。实验结果表明：相比于传统共面电极芯片结构，该芯片结构可将器件的微分电阻降低约75%；当注入电流从1.2倍阈值电流增大到2.8倍阈值电流时，激射波长红移量减少了约77%，特征温度由27.2 K提高到43.4 K，斜率效率增大了约26.4%，最大光电转换效率增大了约4.7倍。所设计的芯片结构方案为制作高性能硅基外延激光器提供了一种优化的技术途径。

关键词 激光器；硅基激光器；直接外延；对称负极结构；微分电阻

中图分类号 TN365 **文献标志码** A **DOI**：10.3788/CJL221277

1 引 言

随着信息化社会的快速发展，信息技术由电子时代迈入光子时代，光互连带来的超快处理速率和超大带宽成为当前乃至未来一段时期的标志[1-2]。与此同时，用于光互连的高性能探测器、调制器[3-4]等器件都已实现了硅基光电集成，而作为光源的半导体激光器仍然是硅基光电集成技术面临的巨大挑战[5]。目前，在Ⅲ-Ⅴ族衬底和带有偏角的Si(001)衬底上制作半导体激光器已取得重大进展[6-9]；然而，带有偏角的Si衬底无法与互补金属氧化物半导体(CMOS)工艺兼容。此外，在Ⅲ-Ⅴ族衬底上制作的激光器可以采用键合的方式实现硅基光电集成，基于键合方案的硅基激光器是目前实现硅光集成芯片的最可行方案，而异质外延是最有希望实现大面积硅光集成和降低成本[10-12]的方案之一。在此背景下，将Ⅲ-Ⅴ族半导体激光器以异质外延的方式直接生长在Si衬底上的方法得到了飞速发展，并受到了国内外的广泛关注。

直接外延硅基激光器是将Ⅲ-Ⅴ族材料外延生长在Si衬底上得到的。由于Si和Ⅲ-Ⅴ族材料之间存在晶格失配、热膨胀系数失配和极性失配等问题，在外延生长时往往会引入穿透位错(TDs)、热裂纹和反相畴(APDs)等缺陷[13]。其中，反相畴缺陷可以通过引入GaP缓冲层[14]、氢化热退火[15-16]、图形化衬底[17]等方法解决，而减少穿透位错和热裂纹的相关研究也在近年来取得了重大进展[18]。在此基础上，Chen等[8]于2016年通过在4°偏角Si(001)衬底上直接外延GaAs(其穿透位错密度低至10^5 cm^{-2})制作了1.3 μm波段的量子点激光器，该器件的微分电阻为2.1 Ω，最大输出功率可达105 mW。2017年，Liu等[19]在GaP/Si衬底上直接外延GaAs(其穿透位错密度为3×10^8 cm^{-2})，实现了室温连续激射的量子点激光器，该器件的微分电阻为4 Ω，最大输出功率为110 mW。值得一提的是，这里采用的芯片结构需要在脊形侧壁沉积Al_2O_3(限制光场)，同时还需要多次沉积SiO_2[20]。2017年，Jung等[21]通过加入位错阻挡层将位错降至7.3×10^6 cm^{-2}，实现了室温连续激射量子点激光器，该激光器的微分电阻为3.4 Ω，输出光功率高达175 mW。同年，Chen等[22]通过氢化热退火去除反相畴，实现了室温连续激射无偏角硅基量子点激光器，该激光器的微分电阻为2.9 Ω，输出功率为43 mW。2018年，Wang等[9]在4°偏角Si(001)衬底上直接外延GaAs(其穿透位错密度为3×10^6 cm^{-2})，并以GaInP为上限制层，实现了室温连续激射的量子点激光器，该激光器的微分电阻为2.8 Ω，

收稿日期：2022-09-27；**修回日期**：2022-11-27；**录用日期**：2022-12-05；**网络首发日期**：2022-12-20

基金项目：国家自然科学基金(61874148)、国家重点研发计划重点专项课题(2018YFB2200104)、北京市科技计划课题(Z191100004819012)、国家创新研究群体科学基金(62021005)、信息光子学与光通信国家重点实验室(北京邮电大学)基金(IPOC2022ZZ01)、高校学科创新引智计划(BP0719012)、北京邮电大学研究生创新创业项目(2022-YC-T031)

通信作者：*wangjun12@bupt.edu.cn

输出光功率为 21.8 mW。2019 年，Shang 等[20]采用 V 型槽去除反相畴，获得了穿透位错密度为 3×10^{6} cm^{-2} 的 GaAs 材料，进而制作了室温连续激射量子点激光器，该激光器的微分电阻为 2.7 Ω，输出光功率为 75 mW。2020 年，Wan 等[23]在 GaP/Si(001)衬底上直接外延 GaAs(其穿透位错密度为 3×10^{7} cm^{-2})，成功实现了室温下可连续激射的量子点激光器，该激光器的微分电阻为 6.5 Ω，输出光功率为 52 mW。2020 年，Wang 等[24]采用 U 型槽消除反相畴，获得了穿透位错密度为 5×10^{6} cm^{-2} 的高质量 GaAs 材料，并制作了锁模量子点激光器[25]，该激光器的微分电阻为 14.5 Ω，输出光功率为 9 mW。同年，Shang 等[18]通过引入非对称位错阻挡层和应变捕获层[26]获得了穿透位错密度低至 1.5×10^{6} cm^{-2} 的 GaAs 材料，并实现了长寿命量子点激光器[27]，该激光器的输出光功率为 65 mW。2022 年，肖春阳等[28]以改善外延材料质量为目标开展相关研究，之后采用氢化热退火消除反相畴[15]，以 GaInP 为上限制层，实现了可室温连续激射的无偏角硅基量子点激光器[29]，该激光器的微分电阻为 7.2 Ω，输出光功率为 63.9 mW。2021 年，Ko 等[30]成功实现了室温连续激射硅基量子阱激光器，该激光器的微分电阻为 2.8 Ω，输出功率为 19.7 mW。

综上所述，提高外延材料质量是改善硅基激光器性能的主要有效方法，但目前鲜有以优化芯片结构、工艺流程等其他途径提升激光器性能的报道。芯片结构和工艺对激光器的模式特性、微分电阻等有直接影响[31]。硅基激光器的微分电阻与器件性能紧密相关。过大的微分电阻会使器件的发热量较大，大幅降低器件的光电转换效率，甚至会使器件无法激射。此外，微分电阻对激光器的输出功率、波长稳定性、斜率效率及可靠性也会有直接影响[32-34]。因此，降低硅基激光器的微分电阻是大幅改善激光器性能的重要措施，同时也是制作高性能硅基激光器的必要条件。

本文提出了一种用于降低硅基激光器芯片微分电阻的对称负极芯片结构(SCS)，该结构的电极更加紧凑，且不必在有源区侧壁沉积 Al_2O_3 限制光场，也无须多次沉积 SiO_2。本课题组在无偏角 Si(001)衬底上制作了不同芯片结构的量子点激光器芯片，并对器件性能进行了对比分析。与传统电极芯片结构(CCS)相比，优化的对称负极芯片结构使激光器芯片的微分电阻降低了约 75%，相应地，激光器性能因此得到显著提升：最大单面输出光功率为 70 mW，最大光电转换效率约提升 4.7 倍，斜率效率约提高 26.4%，特征温度约提高 59.6%。结果表明，该芯片结构可以显著提升激光器的性能，为实现高性能、长寿命硅基激光器提供了一种优化的技术方案。

2 芯片结构及制作

2.1 材料结构

采用金属有机化合物气相沉积(MOCVD)和分子束外延(MBE)两种技术完成量子点激光器材料的外延生长。首先采用 MOCVD 在无偏角 Si(001)衬底上外延生长 2.8 μm GaAs，以消除极性失配带来的反相畴，同时减少 GaAs 材料的穿透位错；接着采用 MBE 生长如图 1(a)所示的材料结构，其中 n 型接触层和 p 型接触层的掺杂浓度分别为 4×10^{18} cm^{-3} 和 2×10^{19} cm^{-3}，下波导层和上波导层的掺杂浓度分别为 1×10^{18} cm^{-3} 和 1×10^{18} cm^{-3}[29]。完成材料的外延生长后，采用扫描透射电镜(STEM)对量子点激光器芯片进行表征，表征结果如图 1(b)所示。这里采用 6 个周期的 InAs/GaAs 量子点作为有源区，测得有源区的光致发光(PL)光谱如图 1(c)所示，其峰值波长为 1312 nm。插图为量子点(QDs)的原子力显微镜(AFM)表征图(1 μm×1 μm)，测得量子点的密度为 4×10^{10} cm^{-2}。

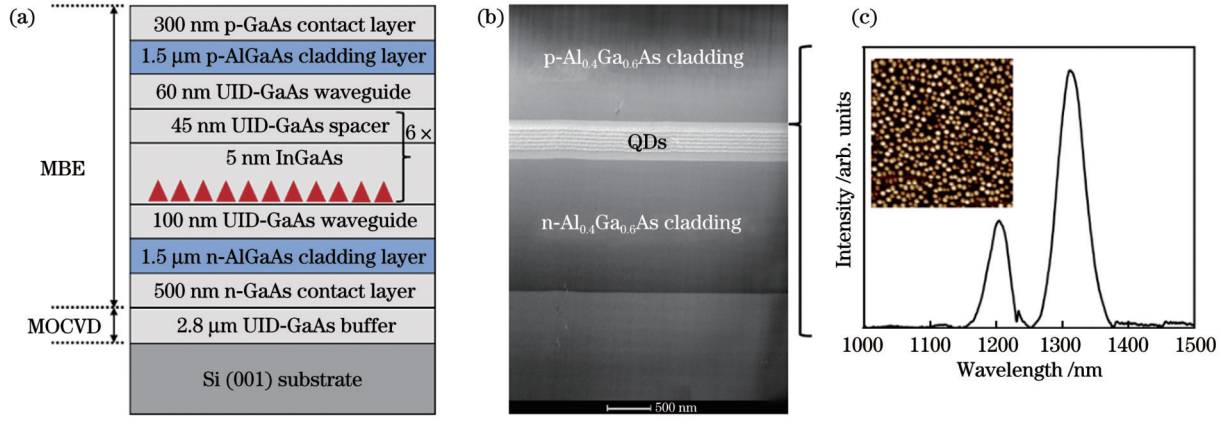

图 1 量子点激光器的外延结构及材料表征。(a)外延结构图；(b)扫描透射电镜(STEM)表征图；(c)量子点的光致发光(PL)光谱，其中插图为量子点的 AFM 表征图(1 μm×1 μm)

Fig. 1 Epitaxial structure and material characterization of the quantum dot laser. (a) Epitaxial structure; (b) scanning transmission electron microscopy (STEM) image; (c) photoluminescence (PL) spectrum of the quantum dots, where the inset is atomic force microscopy (AFM) image of the quantum dots measured within an area of 1 μm×1 μm

2.2 芯片结构及制作

激光器微分电阻的大小决定了器件的发热程度，发热严重时将导致激光器的激射波长发生较大红移，甚至导致激光器无法激射。因此，减小微分电阻不仅可以降低器件的发热程度从而减缓器件劣化，还可以显著提升激光器的光学性能。

对于硅基激光器而言，传统共面电极芯片的截面如图 2(a)所示。将图中电流流向为垂直方向的部分等效为电阻 R_1，将电流流向为水平方向的部分等效为电阻 R_2，则芯片的等效电路如图 2(b)所示。激光器的微分电阻主要来源于电阻 R_2，因此，在缩短电极之间横向距离的同时，采用图 3 所示的对称负极芯片制作量子点激光器。此时，激光器芯片的截面和等效电路分别如图 2(c)和图 2(d)所示，有源区两侧的电阻以并联形式连接。相比图 2(b)所示的传统电极结构的等效电路，图 2(d)所示的等效电路可使器件的微分电阻减小约 50%。此外，该芯片无须在有源区侧壁沉积额外的材料来限制光场，只需预先在 n 型接触层和 p 型接触层沉积金属电极，就可以确保整个激光器的腔长都可以注入电流。所以，只需沉积一次 SiO_2 即可完成激光器的制作，不仅简化了工艺流程，还大幅减小器件的微分电阻。

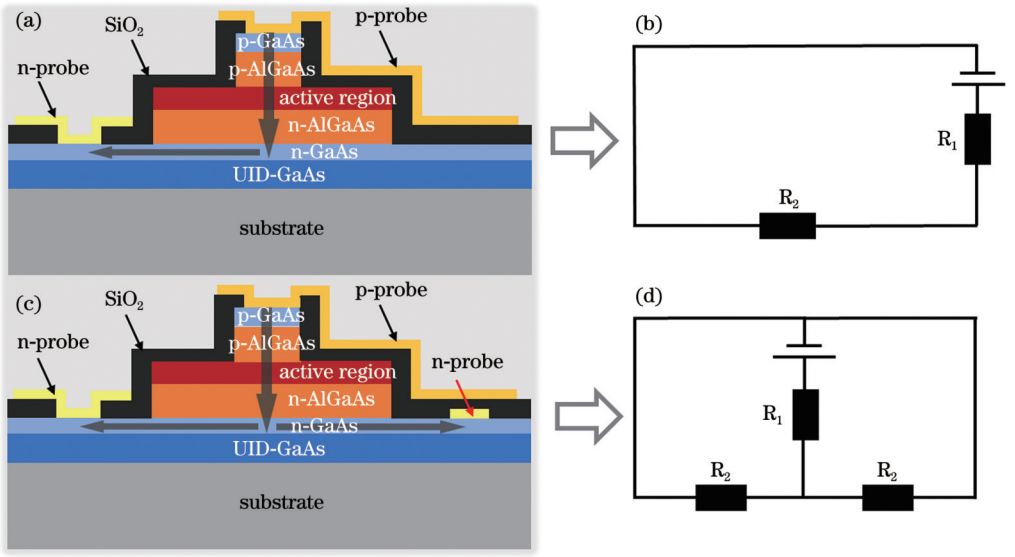

图 2 激光器截面示意图及等效电路。(a)传统电极结构示意图；(b)传统电极结构的等效电路；(c)对称负极结构示意图；(d)对称负极结构的等效电路

Fig. 2 Cross-sectional schematic of the laser and equivalent circuit. (a) Schematic of the conventional cathode structure; (b) equivalent circuit of the conventional cathode structure; (c) schematic of the symmetrical cathode structure; (d) equivalent circuit of the symmetrical cathode structure

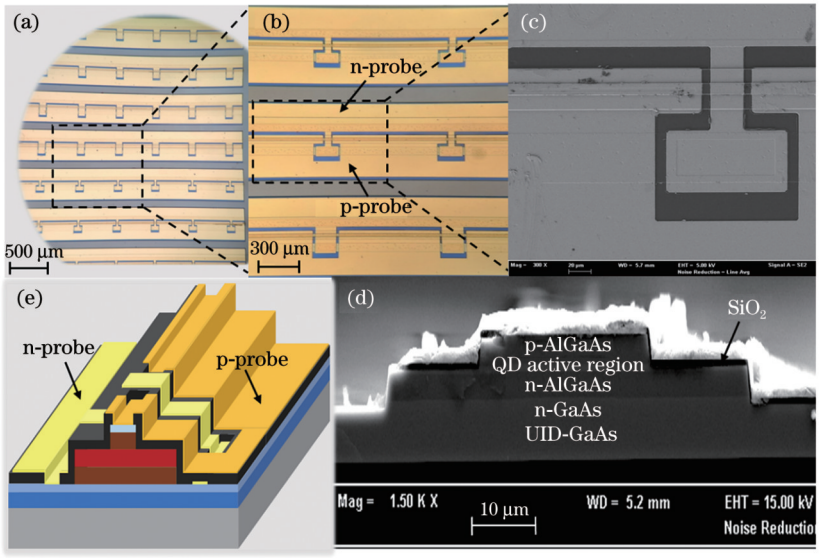

图 3 芯片结构图。(a)(b)不同放大倍数下芯片的平面图；(c)芯片的平面 SEM 图；(d)芯片的截面 SEM 图；(e)芯片的三维结构示意图

Fig. 3 Structural schematic of the chip. (a)(b) Plan-view image of the chip with various scale bars; (c) plan-view SEM image of the chip; (d) cross-sectional SEM image of the chip; (e) three-dimensional structural schematic of the chip

完成激光器芯片材料的外延生长后，采用相同的外延材料和两种不同的芯片结构制作量子点激光器。首先采用感应耦合等离子体刻蚀技术刻蚀出脊状台面，然后采用电子束蒸发方法沉积 Ti/Pt/Au 和 AuGe/Ni/Au（分别作为 p 和 n 接触电极），接着采用等离子增强化学气相沉积技术沉积 300 nm SiO_2 作为电极隔离层，最后沉积金属电极并解理出不同尺寸的激光器芯片。这里制作的激光器芯片腔面均未镀膜。

3　分析与讨论

在室温连续条件下，对制作的硅基量子点激光器的主要性能进行测试分析，其光功率-电流-电压（*L*-*I*-*V*）特性及光谱特性如图 4 所示。图中所示激光器采用对称负极芯片结构制作而成，该激光器的阈值电流密度为 496 A/cm^2，最大单面输出光功率为 70 mW，微分电阻为 1.52 Ω。此外，还对采用传统电极芯片结构制作的硅基激光器的性能进行了对比测试，不同结构激光器的电流-电压（*I*-*V*）特性如图 5（a）所示。当注入电流相同时，传统电极芯片结构制作的硅基激光器的电压约为对称负极芯片结构制作的硅基激光器的 3.8 倍。图 5（b）是不同芯片结构的硅基激光器的微分电阻，可见，对称负极芯片结构大幅降低了激光器的微分电阻。

激光器微分电阻的大小直接影响激光器的发热量和有源区的温升，而激光器的激射波长会随着激光器有源区温升发生红移，导致激光器的波长稳定性下降。图 5（c）给出了不同电流下多个激光器的激射波长，可

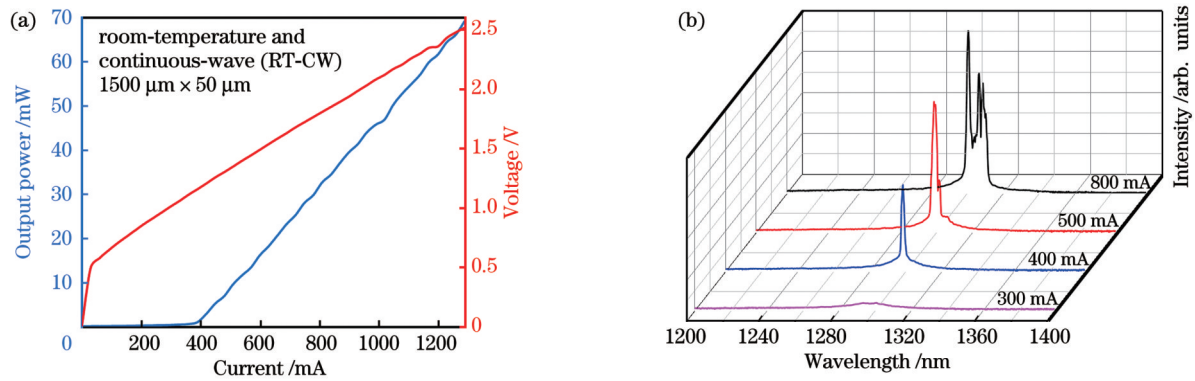

图 4　量子点激光器的表征。（a）光功率-电流-电压特性；（b）光谱特性

Fig. 4　Characteristics of the quantum dot laser. (a) Light-current-voltage characteristics; (b) spectral characteristics

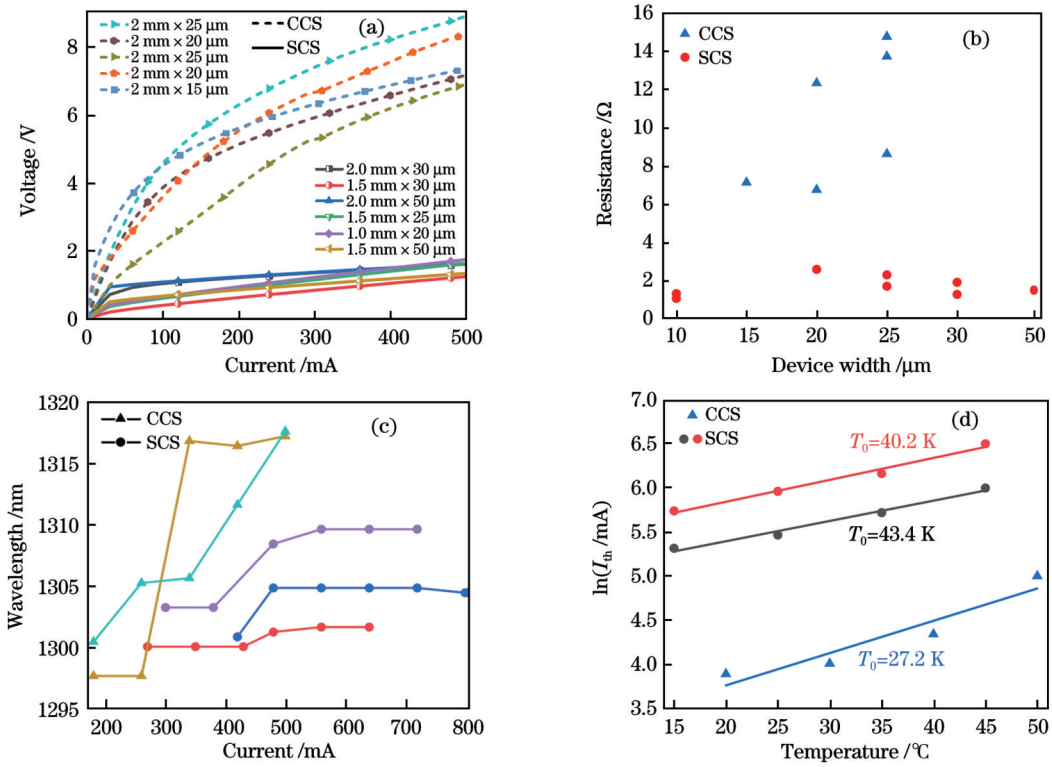

图 5　不同结构激光器的性能对比。（a）电流-电压特性；（b）微分电阻；（c）不同电流下的激射波长；（d）温度特性

Fig. 5　Performance comparison of the lasers with different structures. (a) Current-voltage characteristics; (b) differential resistance; (c) lasing wavelength at different currents; (d) temperature characteristics

见，随着注入电流从1.2倍阈值电流增大到2.8倍阈值电流，传统电极芯片结构激光器的激射波长因发热而红移了约18.4 nm，而采用对称负极芯片结构制作的激光器在相同电流范围内仅红移了约4.1 nm。这表明对称负极芯片结构可通过降低微分电阻使激光器的波长稳定性得到显著提高。图5(d)直接体现出对称负极芯片结构激光器的特征温度在相同工作温度范围内比传统电极芯片结构激光器的特征温度提升了约59.6%(由27.2 K提高到43.4 K)。可见，采用对称负极芯片结构可以提高硅基激光器的波长稳定性，从而显著提升了器件的温度稳定性，为制作高性能硅基激光器提供了一种优化的技术方案。

图6(a)表示不同结构下多个硅基量子点激光器的光电转换效率。可以看出，与传统电极芯片结构制作的激光器相比，采用对称负极芯片结构制作的硅基激光器的光电转换效率显著提升，其最大光电转换效率平均增大了约4.7倍。此外，本文还对硅基量子点激光器的斜率效率和最大单面输出光功率进行了对比，结果如图6(b)所示。与采用传统电极芯片结构制作的硅基激光器相比，采用对称负极芯片结构制作的硅基激光器的斜率效率提高了约26.4%，最大输出光功率则相应增加了4.5倍。

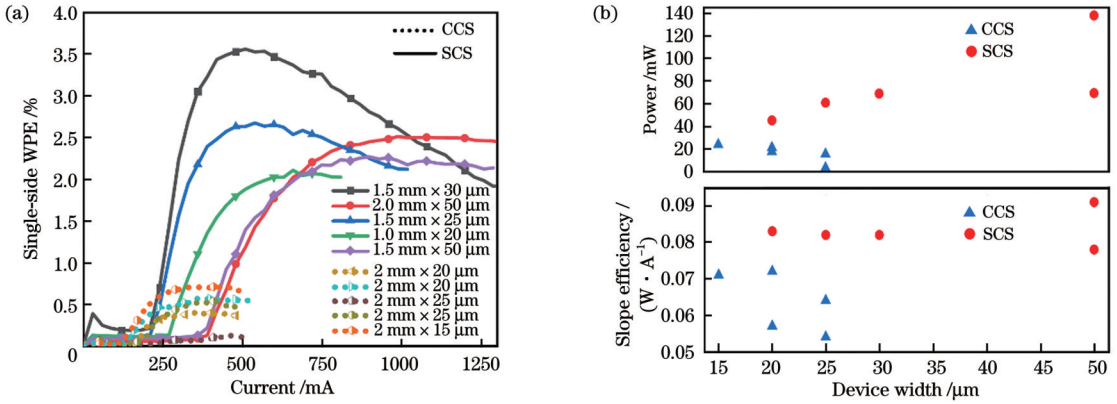

图6　不同结构激光器的性能对比。(a)光电转换效率；(b)斜率效率及最大单面输出功率

Fig. 6　Performance comparison of the lasers with different structures. (a) Wall-plug-efficiency (WPE); (b) slope efficiency and maximum single-side output power

综上，不同电极结构对硅基激光器芯片性能的影响非常显著，而相同电极结构的激光器的尺寸对其性能的影响很小，几乎可以忽略。因此，本文着重分析电极结构对激光器芯片的影响。另外，较低的微分电阻可使激光器性能显著提升，这是由于器件不会因发热量大而导致激光器性能下降，进而大幅提升了激光器的光电性能。

本文对近5年国内外报道的硅基量子点激光器的欧姆接触层及其微分电阻进行了对比，如表1所示。不难看出，本课题组制作的量子点激光器的微分电阻是近年来报道的量子点激光器的最低值，这有利于制作低阈值、大功率、高稳定性以及高可靠性的硅基激光器。

4　结　　论

本文提出了一种用于硅基激光器的对称负极芯片结构，并采用该结构实现了无偏角硅基量子点激光

表1　硅基激光器的芯片尺寸、n型接触层厚度、微分电阻及掺杂浓度比较

Table 1　Chip size, n-contact layer thickness, differential resistance and doped concentration of each silicon-based laser

Year	Chip size /(μm×μm)	n-contact layer thickness /nm	Resistance /Ω	Doped concentration /cm^{-3}	Ref.
2017	750×4		4		[19]
2017	1485×2.5	700	3.4		[21]
2017	3000×25	300	2.9	6×10^{18}	[22]
2018	1079×2.5	700	3.8		[35]
2018	2000×15	500	2.8	5×10^{18}	[9]
2019	1450×10 1450×2	800	2.7 5	2×10^{18}	[20]
2020	1270×5	500	6.5	5×10^{18}	[23]
2021	2500×4	600	14.5		[25]
2022	2000×20	500	7.2	4×10^{18}	[29]
2022	1500×50 2000×30	500	1.29 1.52	4×10^{18}	This work

器的室温连续激射，同时探究了微分电阻对激光器性能的影响。结果表明，采用对称负极芯片结构制作的量子点激光器的微分电阻仅为 1.52 Ω，是迄今为止已报道的硅基激光器电阻的最小值。与采用传统电极芯片结构制作的硅基激光器相比，采用该结构的硅基激光器的特征温度约提高了 59.6%，斜率效率约增大了 26.4%，光电转换效率约提高了 4.7 倍，而且其输出功率达到 70 mW，波长稳定性也得到了显著提升。

通过降低激光器的微分电阻可以显著提升激光器的性能，从而为提升激光器性能提供了另一种重要途径：从优化芯片结构和制作工艺方面提升激光器性能。本文为实现高性能和长寿命硅基激光器提供了一种优化的技术方案。

参 考 文 献

[1] Ho R, Mai K W, Horowitz M A. The future of wires[J]. Proceedings of the IEEE, 2001, 89(4): 490-504.

[2] Davis J A, Venkatesan R, Kaloyeros A, et al. Interconnect limits on gigascale integration (GSI) in the 21st century[J]. Proceedings of the IEEE, 2001, 89(3): 305-324.

[3] Komljenovic T, Huang D N, Pintus P, et al. Photonic integrated circuits using heterogeneous integration on silicon[J]. Proceedings of the IEEE, 2018, 106(12): 2246-2257.

[4] Zhou Z P, Tu Z J, Li T T, et al. Silicon photonics for advanced optical interconnections[J]. Journal of Lightwave Technology, 2015, 33(4): 928-933.

[5] Giewont K, Nummy K, Anderson F A, et al. 300-mm monolithic silicon photonics foundry technology[J]. IEEE Journal of Selected Topics in Quantum Electronics, 2019, 25(5): 8200611.

[6] Sato S, Satoh S. 1.21 μm continuous-wave operation of highly strained GaInAs quantum well lasers on GaAs substrates[J]. Japanese Journal of Applied Physics, 1999, 38(9A): L990-L992.

[7] Lott J A, Ledentsov N N, Ustinov V M, et al. InAs-InGaAs quantum dot VCSELs on GaAs substrates emitting at 1.3 μm[J]. Electronics Letters, 2000, 36(16): 1384-1385.

[8] Chen S M, Li W, Wu J, et al. Electrically pumped continuous-wave III-V quantum dot lasers on silicon[J]. Nature Photonics, 2016, 10(5): 307-311.

[9] Wang J, Hu H Y, Yin H Y, et al. 1.3 μm InAs/GaAs quantum dot lasers on silicon with GaInP upper cladding layers[J]. Photonics Research, 2018, 6(4): 321-325.

[10] 吕尊仁, 张中恺, 王虹, 等. 1.3 μm半导体量子点激光器的研究进展[J]. 中国激光, 2020, 47(7): 0701016.
Lü Z R, Zhang Z K, Wang H, et al. Research progress on 1.3 μm semiconductor quantum-dot lasers[J]. Chinese Journal of Lasers, 2020, 47(7): 0701016.

[11] 李南果, 刘灿, 张鹏斐, 等. 850 nm单模面发射分布反馈式激光器[J]. 中国激光, 2022, 49(12): 1201006.
Li N G, Liu C, Zhang P F, et al. 850 nm single-mode surface-emitting distributed feedback lasers[J]. Chinese Journal of Lasers, 2022, 49(12): 1201006.

[12] 宁永强, 陈泳屹, 张俊, 等. 大功率半导体激光器发展及相关技术概述[J]. 光学学报, 2021, 41(1): 0114001.
Ning Y Q, Chen Y Y, Zhang J, et al. Brief review of development and techniques for high power semiconductor lasers[J]. Acta Optica Sinica, 2021, 41(1): 0114001.

[13] Zhou Z P, Yin B, Michel J. On-chip light sources for silicon photonics[J]. Light: Science & Applications, 2015, 4(11): e358.

[14] Németh I, Kunert B, Stolz W, et al. Heteroepitaxy of GaP on Si: correlation of morphology, anti-phase-domain structure and MOVPE growth conditions[J]. Journal of Crystal Growth, 2008, 310(7/8/9): 1595-1601.

[15] Chen W R, Wang J, Zhu L N, et al. Theoretical and experimental study on epitaxial growth of antiphase boundary free GaAs on hydrogenated on-axis Si(001) surfaces[J]. Journal of Physics D: Applied Physics, 2021, 54(44): 445102.

[16] Martin M, Caliste D, Cipro R, et al. Toward the III-V/Si co-integration by controlling the biatomic steps on hydrogenated Si (001)[J]. Applied Physics Letters, 2016, 109(25): 253103.

[17] Wei W Q, Wang J H, Zhang B, et al. InAs QDs on (111)-faceted Si (001) hollow substrates with strong emission at 1300 nm and 1550 nm[J]. Applied Physics Letters, 2018, 113(5): 053107.

[18] Shang C, Selvidge J, Hughes E, et al. A pathway to thin GaAs virtual substrate on on-axis Si (001) with ultralow threading dislocation density[J]. Physica Status Solidi (A), 2020, 218(3): 2000402.

[19] Liu A Y, Peters J, Huang X, et al. Electrically pumped continuous wave 1.3 μm quantum dot lasers epitaxially grown on on -axis (001) GaP/Si[J]. Optics Letters, 2017, 42(2): 338-341.

[20] Shang C, Wan Y T, Norman J C, et al. Low-threshold epitaxially grown 1.3-μm InAs quantum dot lasers on patterned (001) Si[J]. IEEE Journal of Selected Topics in Quantum Electronics, 2019, 25(6): 1502207.

[21] Jung D, Norman J, Kennedy M J, et al. High efficiency low threshold current 1.3 μm InAs quantum dot lasers on on-axis (001) GaP/Si[J]. Applied Physics Letters, 2017, 111(12): 122107.

[22] Chen S M, Liao M Y, Tang M C, et al. Electrically pumped continuous-wave 1.3 μm InAs/GaAs quantum dot lasers monolithically grown on on-axis Si (001) substrates[J]. Optics Express, 2017, 25(5): 4632-4639.

[23] Wan Y T, Shang C, Norman J, et al. Low threshold quantum dot lasers directly grown on unpatterned quasi-nominal (001) Si[J]. IEEE Journal of Selected Topics in Quantum Electronics, 2020, 26(2): 1900409.

[24] Wei W Q, Wang J H, Zhang J Y, et al. A CMOS compatible Si template with (111) facets for direct epitaxial growth of Ⅲ-Ⅴ materials[J]. Chinese Physics Letters, 2020, 37(2): 024203.

[25] Wang Z H, Wei W Q, Feng Q, et al. InAs/GaAs quantum dot single-section mode-locked lasers on Si (001) with optical self-injection feedback[J]. Optics Express, 2021, 29(2): 674-683.

[26] Selvidge J, Norman J, Hughes E T, et al. Defect filtering for thermal expansion induced dislocations in Ⅲ-Ⅴ lasers on silicon[J]. Applied Physics Letters, 2020, 117(12): 122101.

[27] Shang C, Hughes E, Wan Y T, et al. High-temperature reliable quantum-dot lasers on Si with misfit and threading dislocation filters [J]. Optica, 2021, 8(5): 749-754.

[28] 肖春阳, 王俊, 李家琛, 等. 分子束外延 GaAs/Si(001)材料反相畴的湮灭机理[J]. 中国激光, 2022, 49(23): 2301006.
Xiao C, Wang J, Li J, et. al. Annihilation mechanism of antiphase domain in GaAs/Si (001) materials by molecular beam epitaxy[J]. Chinese Journal of Lasers, 2022, 49(23): 2301006.

[29] Wang J, Liu Z L, Liu H, et al. High slope-efficiency quantum-dot lasers grown on planar exact silicon (001) with asymmetric waveguide structures[J]. Optics Express, 2022, 30(7): 11563-11571.

[30] Ko Y H, Kim K J, Han W S. Monolithic growth of GaAs laser diodes on Si(001) by optimal AlAs nucleation with thermal cycle annealing[J]. Optical Materials Express, 2021, 11(3): 943-951.

[31] Jung C, Jäger R, Grabherr M, et al. 4.8 mW singlemode oxide confined top-surface emitting vertical-cavity laser diodes[J]. Electronics Letters, 1997, 33(21): 1790-1791.

[32] Feng M X, Zhang S M, Jiang D S, et al. Thermal analysis of GaN laser diodes in a package structure[J]. Chinese Physics B, 2012, 21(8): 084209.

[33] Wang Z Q, Sheng Z, Li H, et al. A thermal-optimal design of SOI-integrated microdisk lasers[J]. Optical and Quantum Electronics, 2015, 47(2): 453-461.

[34] Dyment J C, Cheng Y C, SpringThorpe A J. Temperature

dependence of spontaneous peak wavelength in GaAs and $Ga_{1-x}Al_xAs$ electroluminescent layers[J]. Journal of Applied Physics, 1975, 46(4): 1739-1743.

[35] Jung D, Zhang Z Y, Norman J, et al. Highly reliable low-threshold InAs quantum dot lasers on on-axis (001) Si with 87% injection efficiency[J]. ACS Photonics, 2018, 5(3): 1094-1100.

Improved Performances of Lasers on Silicon (001) with Symmetrical Cathode Structures

Ma Bojie[1], Wang Jun[1*], Liu Hao[1], Jiang Chen[1], Liu Zhuoliang[1], Zhai Hao[1], Li Jian[2], Ming Rui[1], Ge Qing[1], Lin Feng[1], Liu Kai[1], Wang Qi[1], Wei Xin[2], Huang Yongqing[1], Ren Xiaomin[1]

[1]*State Key Laboratory of Information Photonics and Optical Communications, Beijing University of Posts and Telecommunications, Beijing* 100876, *China*;

[2]*Institute of Semiconductors, Chinese Academy of Sciences, Beijing* 100083, *China*

Abstract

Objective Investigations of silicon-based optoelectrical integration have become a development trend for an increased transmission rate in optical networks. Currently, most photonic devices achieve on-chip integration, except for silicon-based lasers, which are essential light sources. Heterogeneous epitaxial growth has been used to construct silicon-based Ⅲ-Ⅴ semiconductor laser structures, and it is one of the most promising solutions offering high yield and low costs. Significant efforts have been made to enhance the performance of silicon-based lasers by improving the quality of the as-grown material. However, only a few studies have been conducted on optimizing the laser-chip structure and the fabrication process that directly influences the lasing modes, differential resistances, and other properties of the lasers. Moreover, high differential resistance can reduce the output power, slope efficiency, and wall-plug efficiency (WPE) of the lasers and can even cause lasing failure owing to excessive waste heat. Therefore, reducing the differential resistance of silicon-based lasers is critical for significantly improving laser performance and realizing high-performance silicon-based lasers.

Methods Combined with the advantages of metalorganic chemical vapor deposition (MOCVD) and molecular beam epitaxy (MBE), the quantum-dot (QD) laser structure was grown on a two-inch complementary metal-oxide semiconductor (CMOS)-compatible Si (001) substrate (Fig. 1). Moreover, Fabry-Perot (F-P) laser devices were fabricated using two different chip structures. The ridges were etched using inductively coupled plasma (ICP) via standard photolithography. Ti/Pt/Au and AuGe/Ni/Au were deposited via physical vapor deposition (PVD) as p- and n-type contact electrodes, respectively. A 300 nm thick SiO_2 layer was deposited via plasma-enhanced chemical vapor deposition (PECVD) for electrical isolation. The as-fabricated wafers were fabricated into different chip sizes by adequate cleaving and then mounted on Cu heatsinks with C-mount packages. Finally, the main performance of the lasers with these two chip structures was determined for further comparison and analysis.

Results and Discussions The main performance of the silicon-based quantum dot laser was determined under CW conditions at room temperature (25 ℃). The F-P lasers, each with a cavity length of 1.5 mm and a stripe width of 50 μm, achieve a single-facet output power of 70 mW and differential resistance of 1.52 Ω (Fig. 4). The voltage of the lasers with the conventional cathode structure is approximately 3.8 times that with the symmetrical cathode structure under the same injection currents (Fig. 5). The lasing wavelength of the lasers with conventional cathode structure exhibits a red shift by approximately 18.4 nm owing to additional waste heat, whereas the laser with symmetrical cathode structures exhibits a red shift by only approximately 4.1 nm when the injection current increases from 1.2 to 2.8 times the threshold current (Fig. 5). Moreover, compared with the conventional cathode structure, the symmetrical cathode structure can significantly reduce the device differential resistance by approximately 75%, increasing the characteristic temperature from 27.2 to 43.3 K (Fig. 5). In addition, the slope efficiency and maximum wall-plug efficiency increased by 26.4% and 4.7 times, respectively (Fig. 6).

Conclusions In this study, a new chip structure of lasers on silicon was designed, which could reduce the differential resistance compared with the conventional cathode structure, significantly improving the laser performance. QD lasers on a two-inch CMOS-compatible Si (001) substrate were fabricated using this structure, and the influence of the chip structure on laser performance was investigated experimentally. The results show that the differential resistance of the lasers with symmetrical cathode structures is only 1.52 Ω, which is significantly low differential resistance. Compared with the conventional cathode structure, the chip structure can significantly reduce the differential resistance of the device by approximately 75% and increase the characteristic temperature by approximately 59.6%. In addition, the slope efficiency and maximum wall-plug efficiency increase by 26.4% and 4.7 times, respectively, the output power reaches 70 mW, and the stability improves significantly. In summary, the laser performance can be significantly enhanced by decreasing the differential resistance, which provides another critical approach to enhancing the laser performance and offers an optimized technical solution for producing high-performance and highly reliable lasers on silicon.

Key words lasers; lasers on silicon; direct epitaxy; symmetrical cathode structures; differential resistance